

Helio­stat Field Layout Design for Solar Tower Power Plant Based on GPU^{*}

Yiyi Zhou, Yuhong Zhao

*Department of Control Science and Engineering, Zhejiang University,
Hangzhou, Zhejiang, China, (e-mail: yhzha@iipc.zju.edu.cn)*

Abstract: A new method of helio­stat field layout design is presented for solar tower power plant in this paper. In order to make the best use of a stretch of land, maximizing the product of the annual optical efficiency and the ground coverage is taken as the optimization objective in consideration of the conflict between them on the premise that the mechanical collision of adjacent helio­stats is avoided for the specific land area and mirror size. Due to the large amount of computation, Monte Carlo ray tracing method based on Graphic Processing Unit (GPU) is utilized to calculate the annual optical efficiency of a solar tower power plant with high accuracy in a small amount of computation time. The design methods for two typical layout patterns including cornfield and radial stagger are proposed respectively and the effectiveness of the methods is verified by the optimization results of the field layout.

Keywords: Solar tower power plant, GPU computing, layout design, optical efficiency, ground coverage

1. INTRODUCTION

Solar energy as an important tool against energy crisis is becoming a hot spot of new energy because it is renewable, rich, free to use and non-polluting. Solar tower power system has a broad prospect at the lowest costs of electricity generation in large scale (Zhang et al. (2006)). A solar tower power plant is made up of helio­stats, towers, receivers, heat transfer devices, thermal storage devices and the power generation part. The solar radiation is reflected and gathered by an array of mirrors called helio­stat field to the aperture of one or more receivers to form high-temperature steam in an associated thermodynamic process to promote the turbine power generation. Since the helio­stat field provides the reflected energy and contributes almost half of the total plant cost, the design and optimization of helio­stat field layout is crucially important. Therefore the annual optical efficiency that evaluates the performance of the helio­stat field needs to be calculated repeatedly and accurately.

Many codes and methods have been developed to simulate the optical efficiency of the helio­stat field. First generation codes came from the preliminary studies carried out in the US for Solar One in the late 70s including HELIOS, MIRVAL and DELSOL (Gracia et al. (2008); Gollado and Turegano (1989); Kribus et al. (1998)). Although they are still used today, they can only achieve simple function. For example, HELIOS is not adapted to large helio­stat fields; it can neither assess annual performances, nor optimize helio­stat layout. With the continuous updating of the emulator, currently used codes like FIATLUX, HFLCAL, SOLTRACE are becoming more powerful, but none of them can perform well both on accuracy and speed due

to the large amount of computation that is difficult to be handled on CPU. It is also hard to design helio­stat layout by using them.

Then, as the release of the Compute Unified Device Architecture (CUDA) toolkit by NVIDIA in 2006, Graphic Processing Unit (GPU) has become an integral part of today's mainstream computing system. In this paper, a ray tracing tool based on GPU is developed to calculate the annual optical efficiency in exact physical consideration of cosine effects, shadowing and blocking(S&B) factor, spillage, atmospheric attenuation and mirror reflectivity except mirror imperfections. The method is adapted to any helio­stat field pattern, focusing on a high accuracy in a small amount of computation time. Consequently two typical patterns of helio­stat field layout are designed and optimized on the basis of the fast calculation on GPU.

The paper is organized as follows. The model of the optical efficiency is described in Section 2, along with the idea of Monte Carlo ray tracing method. In Section 3 the implementation on CUDA of the optical efficiency computation is introduced. In section 4, the method of layout design is proposed for two typical modes of helio­stat field. The simulation results of the annual optical efficiency are shown in Section 5 as well as the optimization results of the field layout. Finally, conclusions are drawn and the future research is indicated in Section 6.

2. MODEL OF THE OPTICAL EFFICIENCY

The optical efficiency η_{field} measures the energy loss of the helio­stat field. In general, the optical efficiency of the field can be given by:

$$\eta_{field} = \eta_{mirror} \cdot \eta_{cos} \cdot \eta_{S\&B} \cdot \eta_{int} \cdot \eta_{At.M} \quad (1)$$

where η_{mirror} is mirror reflectivity, η_{cos} is cosine efficiency, $\eta_{S\&B}$ is shadowing and blocking efficiency, η_{int} is spillage

^{*} Supported by the National Science Foundation of China (61173128) and 973 Program of China (2012CB720500).

efficiency, and $\eta_{At.M}$ is atmospheric attenuation efficiency. Among them, the value of mirror reflectivity η_{mirror} depending on the heliostat reflective rate can be set to a constant ($\eta_{mirror} = 0.88$ is adopted here), the others are influenced by the heliostat field configuration, the height of the receiver or other factors related. As a result, four types of efficiency except η_{mirror} need to be computed to determine the optical efficiency.

2.1 The Atmosphere Attenuation Efficiency, $\eta_{At.M}$

The effect that some of the energy of the reflected rays are scattered and absorbed by the atmosphere is referred as atmospheric attenuation loss. The attenuation of solar radiation expressed as Equation 2 (Schmitz et al. (2006)) can be regarded as a function of the distance between each heliostat and the receiver d_{HM} in the case of certain weather condition, and the farther the distance is, the smaller the value of $\eta_{At.M}$ is.

When $d_{HM} \leq 1000m$,

$$\eta_{At.M} = 0.99321 - 1.176 \times 10^{-4}d_{HM} + 1.97 \times 10^{-8}d_{HM}^2$$

otherwise,

$$\eta_{At.M} = e^{-0.0001106 \times d_{HM}} \quad (2)$$

2.2 The Cosine Efficiency, η_{cos}

The cosine efficiency η_{cos} is related to the cosine angle between the incident vectors of sunlight and the normal vectors of the heliostats. The surface of the heliostats is assumed to be perfectly flat, so the normal vector of each heliostat \mathbf{N} is definite. While the incident rays can't be considered parallel because the sun is a disk rather than a point for any observation place on the earth. Thus it's of vital importance to generate the incident rays according to the energy distribution of the sun.

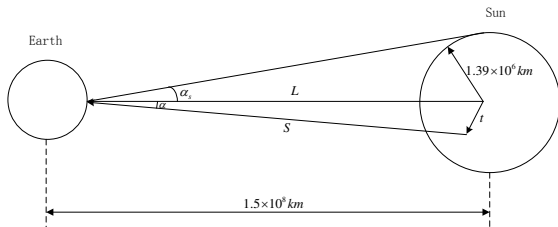


Fig. 1. Solar Angle

Each incident ray has an angle subtended between the center of the sun to some point toward the edge called the solar angle α as shown in Figure 1. The directional vector \mathbf{S} starting from the sun towards the center of the mirror is defined as the incident vector. Every incident ray can be described by an angle α and its energy. Supposing that the value of each ray's energy is same, the flux distribution of the sun could be described by the density of the points as shown in Figure 2, where the closer the points appear to the center of the sun, the greater the number of the points is. Here, one empirical model proposed by Walzel et al. (Walzel et al. (1977)) is selected to evaluate the value of solar energy flux density $S(\alpha)$ for different solar angle α :

$$S(\alpha) = \begin{cases} S_0 \{1 - \lambda(\frac{\alpha}{\alpha_s})^4\} & \alpha \leq \alpha_s \\ 0 & \alpha > \alpha_s \end{cases} \quad (3)$$

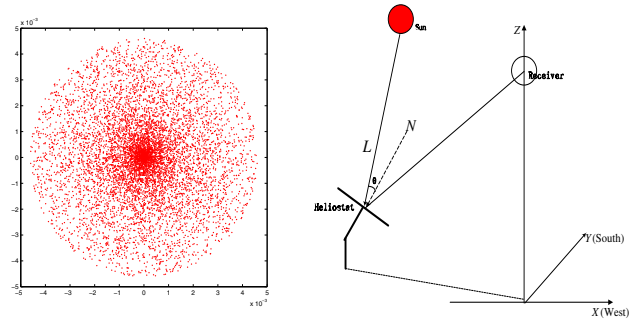


Fig. 2. Solar Flux Density Fig. 3. Cosine Angle

where $\lambda = 0.5138$, α_s is the maximum solar angle and $\alpha_s \approx (1.39 \times 10^6 / 1.5 \times 10^8) / 2 \approx 4.6 mrad$ as shown in Figure 1. S_0 is determined by the distance between the sun and the observation point, and it has the same unit as $S(\alpha)$, W/m^2 . Consequently a large number of rays are produced depending on the probability of the energy flux density by Roulette Wheel Selection Principle. The directional vector \mathbf{S} can be expressed as:

$$\mathbf{S} = \mathbf{L} + \mathbf{t} \quad (4)$$

where \mathbf{L} is defined as the main incident vector when α is set to 0, which is always used while the sunlight is considered as parallel. Let \mathbf{L} and \mathbf{N} with the consistent direction be the unit vector as shown in Figure 3. Thus, the cosine efficiency of each heliostat can be expressed as follows:

$$\eta_{cos} = \cos[\arccos(\mathbf{L} \cdot \mathbf{N})] \quad (5)$$

2.3 The Shadowing and Blocking Efficiency, $\eta_{S\&B}$ and the Spillage Efficiency, η_{int}

The phenomenon that light rays are blocked by adjacent heliostats during the spread is the reason of loss of shadowing and blocking. And the effect that reflected light rays are limited by the size of the receiver causes the spillage. Monte Carlo ray tracing method is adopted to calculate $\eta_{S\&B}$ as well as η_{int} of the whole field, which could easily track the movements of each sunlight and clearly judge out whether light rays intersect the heliostats.

Firstly the projection scope needs to be determined dynamically by calculating the projection coordinates of the center and vertices of the heliostats along the main incident vector on the ground. Then points are cast randomly based on the Monte Carlo method as many as possible to cover the whole projection area of the heliostat field on the ground. A point and a directional vector make up an incident light.

Here ray tracing method is mainly divided into three stages called shadowing, blocking and spillage judgment. The main idea is as follows by taking a random point for instance: Firstly whether the point on behalf of the incident light falls in mirrors is determined according to the projection coordinates of four vertices along the main incident vector on the ground, if not in any mirror, the next point is considered, otherwise judge out which mirror (target mirror) the incident ray is on and mark the intersection coordinates to calculate the corresponding reflected ray; Secondly whether the reflected ray is blocked by other mirrors surrounded is determined, if not, the place

where the reflected ray intersects the receiver plane should be marked; Finally whether the intersection above is in the plane of the heat receiver can be easily determined.

Not until all points cast have been settled, statistical number of shadowed, blocked and spillage rays can be obtained to easily figure out $\eta_{S\&B}$ and η_{int} .

3. CUDA IMPLEMENTATION

In order to obtain the annual optical efficiency of the field, which is based on the hourly performance on certain days during a year, these four types of efficiency have to be simulated at hundreds of solar positions (the azimuth angle and the elevation angle of the sun) for thousands of heliostats leading to a large amount of computations and a long running time(Xie et al. (2012)). Hence, GPU based on standard language C with multi-threaded CUDA design is introduced and used here to accelerate the procedure. GPU was promoted in 1999 by NVIDIA and it was designed purely as accelerators for graphic rendering. However, GPU has evolved into powerful yet affordable parallel floating point co-processors. The realization of parallel computing is accomplished by calling the kernel functions on the device port. GPU's two-layer parallel structure helps us speed up the calculation of optical efficiency, especially $\eta_{S\&B}$ and η_{int} .

In the scope of the work, the workstation is equipped with the NVIDIA GeForce GTX 260 in the Visual Studio 2008 environment under the 32-bit Windows 7 operation system.

NVIDIA Company launched a general parallel computing architecture — CUDA that provides a programming environment and instruction set to solve the problems of complex calculations. The core part of CUDA programming model(NVIDIA (2011)) includes thread system, shared memory and thread synchronization. The CUDA C functions are called kernels organized as a grid of thread blocks, each one executing a certain number of parallel data threads. The tasks of threads inside the same thread block as an isolated problem must be assigned to the same stream processor (SMP), no synchronized communication between these blocks.

The inputs for the developed code are the coordinates of the heliostats, the receiver and the incident rays, which are computed first on CPU port. Each thread on GPU completes the computation of one randomly-cast point independently.

4. HELIOSTAT FIELD LAYOUT DESIGN

The fast simulation of annual optical efficiency based on GPU computing makes it easier to optimize and design the field layout of a solar tower power plant. It has been proved that a close-packed heliostat field with a high ground coverage exhibits more shadowing and blocking(Schramek et al. (2009)). Ground coverage defined as the total area of the heliostats divided by the field area of the given land represents the local density of the heliostats. Thus a higher annual performance can be achieved up to a certain trade-off between the ground coverage and the optical efficiency. Hence, maximizing the product of annual optical efficiency

and the ground coverage is taken as the optimization objective.

During the process of optimization, since there is no explicit function between the decision variables and the optimization objective, the optimization algorithms based on gradient are not appropriate here and the Simplex Search method put forward by Nelder and Mead as a gradient-free algorithm is used. The detail of the Simplex method can be referred to(Nelder and Mead (1965)).

Two typical patterns of field layout including cornfield and radial stagger are designed under a given stretch of land.

4.1 Cornfield Pattern

The main idea of the heliostat field layout design is to locate the receiver and the mirrors in a given land area. Once the column space and line space between the mirrors are determined, the number of the mirrors of each row and column can easily be figured out. Thus a field layout is generated to calculate the corresponding annual optical efficiency and the ground coverage. Table 1 lists the decision variables and their description for cornfield pattern, where H_t is the height of the aim point of the receiver tower, l_m is the length of the heliostat, w_m is the width of the heliostat, h_r is the elevation angle of the reflected vectors of the heliostats.

Table 1. Decision Variables of Cornfield

Decision Variables	Description	Search Range
R_0	The distance between the receiver and the first row	$[0.75H_t, 1.5H_t]$
dx	Column space	$[DM, 2l_m]$
dy	Row space	$[DM, w_m/\sin(h_r)]$

- (1) The lower bound of the decision variables

The lower bound of the search range of column space and line space between mirrors is determined by the safety distance(Siala and Elayeb (2011)) that equals to the diagonal of the heliostat plus the separation distance as follows:

$$DM = \sqrt{l_m^2 + w_m^2} + dS \quad (6)$$

where dS is the separation distance.

- (2) The upper bound of the decision variables

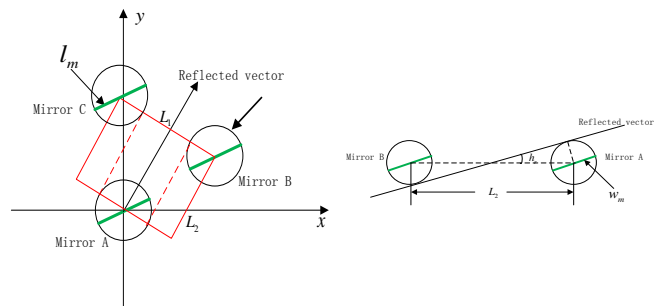


Fig. 4. Top View for No Blocking(Left)
Side View for No Blocking(Right)

In order to reduce the search time, the upper bound of the search range of column space and line space is determined for no blocking(Xie (2013)). As shown in Figure 4(Left), assuming that the projection of the

edge of Mirror B is just tangent to Mirror A's, the line across the center of Mirror B is made perpendicular with L_1 . When the reflected vector is tangent to the equivalent circle of Mirror A and Mirror B, L_1 gets the maximum value: $L_1 = 2l_m$. That means Mirror B won't block Mirror A at any time. According to Figure 4(Right), the length of L_2 can also be determined by $L_2 = w_m / \sin(h_r)$.

4.2 Radial Stagger Pattern

Most heliostat field layout designs take a radial stagger pattern(Lipps and Vant-Hull (1978); Sanchez and Romero (2006)) according to the fact that each heliostat could move freely and the heliostats standing in between two heliostats of the front ring reduce the blocking. Most approaches to improve the layout design of the heliostat field are based on the radial stagger concept. Table 2 lists the decision variables and their description for the radial stagger pattern.

Table 2. Decision Variables of Radial Stagger

Decision Variables	Description	Search Range
R_{coef}	The optimized coefficient of the radius of the ring(from the second ring)	[0, 1]
A_{coef}	The optimized coefficient of the angular direction unit of the ring	[0, 1]

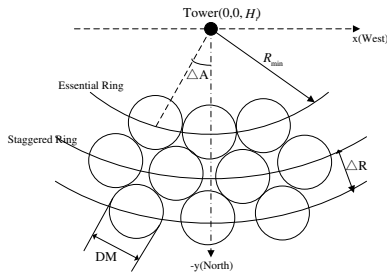


Fig. 5. The Field Layout of Radial Stagger Pattern

- (1) The radius of the first ring Firstly, the following definitions are introduced(Siala and Elayeb (2011)) as shown in Figure 5.

Essential Ring: The rings that have a heliostat on the north axis in the field.

Staggered Ring: The rings that have no heliostat on the north axis in the field.

Here, the radius of the first ring R_0 , by definition an essential ring, is usually given in terms of the aim point height H_t as recommended by Pylkkanen(Pylkkanen (1993)):

$$R_0 = H_t \quad (7)$$

- (2) The lower and upper bound of the radius

The minimum radius of the heliostats should ensure that it does not happen that adjacent heliostats have mechanical collisions. So it satisfies the following conditions as shown in Figure 5:

$$\Delta R_{min} = R_{m+1,min} - R_m = DM \times \cos 30^\circ \times \cos \beta_L \quad (8)$$

where β_L is the tilt angle of the field (β_L is set to 0).

The maximum radius should be determined according to the principle that there is no blocking between the

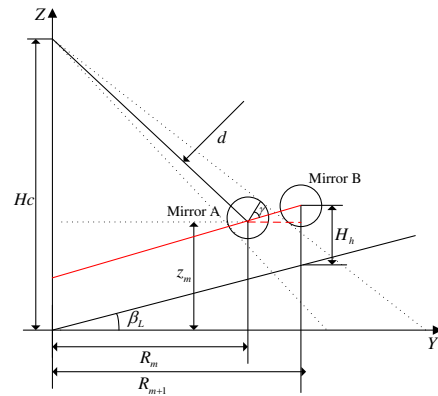


Fig. 6. The Radius for No Blocking

heliostats(Zhang et al. (2009)) as shown in Figure 6. The detail of the calculation is as follows:

$$z_m = R_m \tan \beta_L + H_h \quad (9)$$

$$d = \sqrt{R_m^2 + (H_c - z_m)^2} \quad (10)$$

$$\gamma = \arcsin\left(\frac{DM}{2d}\right) + \arcsin\left(\frac{R_m}{d}\right) - \beta_L \quad (11)$$

$$\Delta R_{max} = R_{m+1,max} - R_m = DM \cos \beta_L / \cos \gamma \quad (12)$$

where H_h is the height of the mirror, and H_c is the height of the tower.

So the the radius of each ring can be expressed as:

$$R_{m+1} = R_m + \Delta R_{min} + R_{coef}(\Delta R_{max} - \Delta R_{min}) \quad (13)$$

where R_{coef} is the optimized coefficient of the radius, $0 < R_{coef} < 1$.

- (3) The lower and upper bound of angular direction unit

Angular direction unit is the angle between the distributions axes. In the paper, the angular direction unit of each ring is assumed to be the same. The minimum value of the angular direction unit is given by:

$$\Delta A_{min} = \arcsin(DM/2/R_m) \quad (14)$$

The maximum value of the angular direction is to avoid blocking. So it is given by:

For the first ring:

$$\Delta A_{max} = \arcsin(DM/2/R_m) + \arcsin(DM/2/R_{m+1}) \quad (15)$$

From the second ring:

$$\Delta A_{max} = \arcsin(DM/2/R_m) + \arcsin(DM/2/R_{m-1}) \quad (16)$$

So the angular direction unit can be expressed as:

$$A_m = \Delta A_{min} + A_{coef}(\Delta A_{max} - \Delta A_{min}) \quad (17)$$

where A_{coef} is the optimized coefficient of the angular direction unit, $0 < A_{coef} < 1$.

Thus the angle between the north axis and the distribution axes can be given by:

$$\psi_m = \pm n A_m \quad (18)$$

where $n = 0, 2, 4, \dots$ is for essential rings, $n = 1, 3, 5, \dots$ is for staggered rings.

The optimal field layout with maximum value of the product of the ground coverage and annual optical efficiency can be obtained through the search of above decision variables.

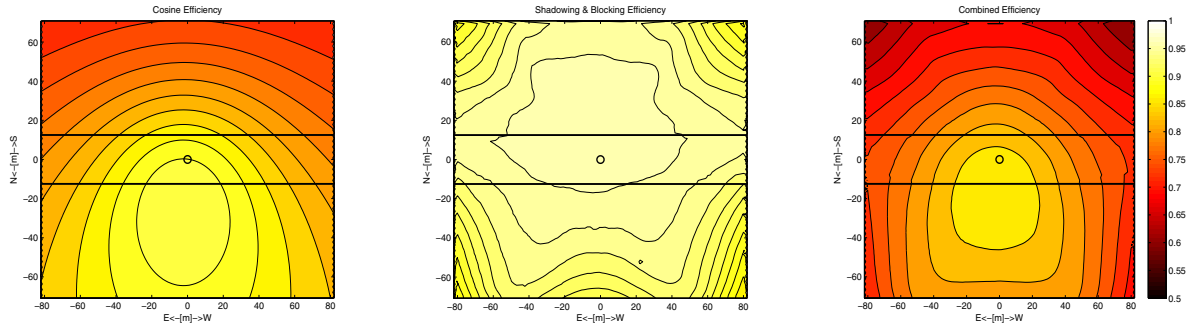


Fig. 7. Annual Optical Efficiency of the Simulated Plant

5. RESULTS

5.1 The Simulation of the Simulated Plant on GPU

The codes are applied to calculate the optical efficiency of a cornfield pattern similar to the eSolar plant located in southern California(Schell (2011))(the number of heliostats is 100×100 , the size of each heliostat is $1.425m \times 0.8m$). Table 3 shows the different running time respectively on CPU and GPU at a certain moment (a certain solar position). The result shows that the computation time on GPU decreases by about 6000 times.

Table 3. Execution Time under CPU and GPU

Points Cast	CPU Time	GPU Time
10^7	10623.5s	1.73s

Here, it must be particularly noted that the field of the simulation field is divided into 100 blocks (10×10) corresponding to 10×10 mirrors each region in the coding design because threads in the same block could exchange data through shared memory including the normal vector, the reflected vector and the vertices coordinates of each heliostat. In order that the coordinate information of the mirrors could be precisely stored in the local memory corresponding to each thread, the number of threads per block is set to 100.

According to the coding design, four arrays, whose size is $100 \times \text{float}$, are used to store the number of the ground rays, the shadowed rays, the blocked rays and the spillage rays of each block. Thus the cosine efficiency, the shadowing and blocking efficiency and the spillage efficiency of each block can be calculated and plotted. The annual optical efficiency of the simulated field is 72.2% compared to the 70.1% of the eSolar plant. The average annual optical efficiency of the field is shown in Figure 7, which is consistent with the reality(Mancini (2000)).

5.2 Results of the Layout Design

Optimal layout of cornfield pattern The optimal field layout of cornfield pattern is shown in Figure 8, and the related details of the field and the optimization results are listed in Table 4.

Optimal layout of radial stagger pattern A heliostat is located in the field by defining the coordinates of its center. These are known once the angular direction of the heliostat

Table 4. The Details and Results of Cornfield

Details of the field	
Latitude	30
Height of the tower	30m
Heliostat size	$1m \times 1m$
Separation distance	0.1m
Field size(the land area the mirrors cover)	$50m \times 50m$
Optimization results	
R_0	22.5m
dx	1.71m
dy	1.51m
Annual optical efficiency	86.3%
Ground coverage	38.3%

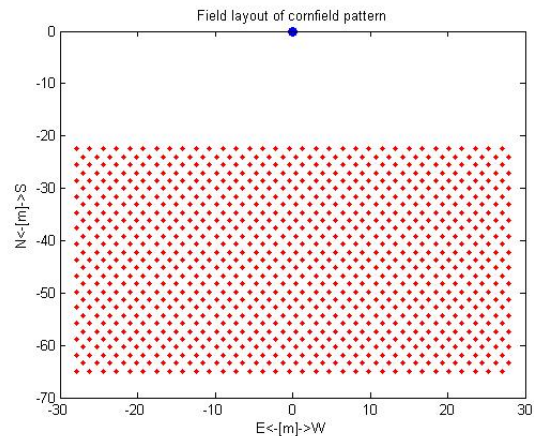


Fig. 8. The Optimal Field Layout of Cornfield Pattern

and the radius of the ring to which it belongs are fixed. So it can be given by:

$$\begin{cases} x = R_m \sin \psi_m \\ y = -R_m \cos \psi_m \\ z = z_m \end{cases} \quad (19)$$

The optimal field layout of radial stagger pattern is shown in Figure 9, and the related details of the field and the optimization results are listed in Table 5, where field size is different from that of the cornfield pattern in that it is the area of the band circle from the radius of the first ring to the given search range of the radius (12m).

As shown in Table 4 and Table 5, the result of annual optical efficiency could reach up to more than 80%, while the optical efficiency of the general field is about 70%(Wei and Lu (2010)). As a result, the overall optical efficiency of the field is raised. On the other hand, the optimal

Table 5. The Details and Results of Radial Stagger

Details of the field	
Latitude	30
Height of the tower	30m
Heliostat size	1m×1m
Separation distance	0.1m
Field size	$\pi/2 \times \{(R_0 + 12)^2 - R_0^2\}$
Optimization results	
Radius of each ring	[30, 31.9, 33.3, 35.3, 36.6, 38.9, 40.6]
Angular direction unit of each ring in radians	[0.0558, 0.0563, 0.0476, 0.0429, 0.05166, 0.0462, 0.0411]
Annual optical efficiency	82.5%
Ground coverage	33.6%

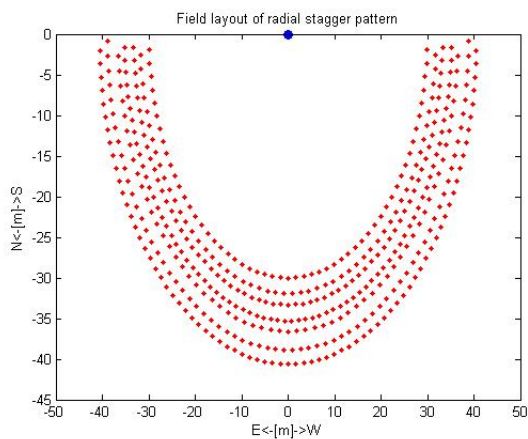


Fig. 9. The Optimal Layout of Radial Stagger Pattern

layout designed in the paper has ground coverage of about 38% and 34%, that is more than those usually have 30%(Schramek et al. (2009)). It is also found that, during the design process, the ground coverage has no obvious relation with the pattern of the heliostat field which affects other costs of the field.

6. CONCLUSION

A new parallel simulation method based on GPU is developed to calculate the annual optical efficiency of a solar tower power plant in this paper. The solar model in consideration of the divergence of the sunlight is built up to be consistent with Monte Carlo ray tracing method. The codes are applicable to various field arrangement and scale, demonstrating that the processing time on GPU can be reduced significantly under the same accuracy. Two typical heliostat field patterns are designed and optimized based on the developed methods presented here. In the process of design, the search distance is ranged from the safety distance to the upper bound for no blocking. The further work will be focused on how to take more constraints and objectives into account.

ACKNOWLEDGEMENTS

The authors acknowledge the financial support of NSFC (61173128) and 973 Program of China (2012CB720500).

REFERENCES

- Gollado, F. and Turegano, J. (1989). Calculation of the annual thermal energy supplied by a defined heliostat field. *Solar Energy*, 42(2), 149–165.
- Gracia, P., Ferriere, A., and Bezian, J. (2008). Codes for solar flux calculation dedicated to central receiver system applications: a comparative review. *Solar Energy*, 82(3), 189–197.
- Kribus, A., Zaibel, R., and et al (1998). A solar-driven combined cycle power plant. *Solar Energy*, 62(2), 121–129.
- Lipps, F. and Vant-Hull, L. (1978). A cellwise method for the optimization of large central receiver systems. *Solar Energy*, 20(6), 505–516.
- Mancini, T.R. (2000). Catalog of solar heliostats. Technical Report 1.
- Nelder, J. and Mead, R. (1965). A simplex method for function minimization. *The Computer Journal*, 7(4), 77–92.
- NVIDIA (2011). *NVIDIA CUDA C Programming Guide*.
- Pylkkanen, T. (1993). *Atlantis Energy LTD*. Personal Communication.
- Sanchez, M. and Romero, M. (2006). Methodology for generation of heliostat field layout in central receiver systems based on yearly normalized energy surfaces. *Solar Energy*, 80(7), 861–874.
- Schell, S. (2011). Design and evaluation of esolars heliostat fields. *Solar Energy*, 85(4), 614–619.
- Schmitz, M., Schwarzbözl, P., Buck, R., and Pitz-Paal, R. (2006). Assessment of the potential improvement due to multiple apertures in central receiver systems with secondary concentrators. *Solar Energy*, 80(1), 111–120.
- Schramek, P., Mills, D., Stein, W., and Lievre, P. (2009). Design of the heliostat field of the csiro solar tower. *Journal of Solar Energy Engineering*, 131(2).
- Siala, F. and Elayeb, M. (2011). Mathematical formulation of a graphical method for a no-blocking heliostat field layout. *Renewable Energy*, 23(1), 77–92.
- Walzel, M., Lipps, F., and Vant-Hull, L. (1977). A solar flux density calculation for a solar tower concentrator using a two-dimensional hermite function expansion. *Solar Energy*, 19(3), 239–253.
- Wei, X. and Lu, Z. (2010). Design and optimization of heliostat field layout for solar tower power plant. *Acta Optica Sinica*, 30(9), 2652–2656(in Chinese).
- Xie, F. (2013). Optical simulation of heliostat field in solar tower power system and its application. *Master thesis of Zhejiang University*.
- Xie, F., Zhao, Y., and Zhou, L. (2012). Fast simulation of annual optical efficiency of solar tower power plant. *Proceedings of 11th International Symposium on Process Systems Engineering*, 555–559.
- Zhang, H., Juchli, I., Favrat, D., and Pelet, X. (2009). Multi-objective thermoeconomic optimisation of the design of heliostat field of solar tower power plants. *Acta Energiae Solaris Sinica*, 30(1), 30–55(in Chinese).
- Zhang, Y., Wang, J., and et al (2006). Series on solar thermal power generation (2) – tower type and rough type solar thermal power generation. *Solar Energy*, 2, 29–32(in Chinese).